

Comparison of Austenite Decomposition Models During Finite Element Simulation of Water Quenching and Air Cooling of AISI 4140 Steel

K. BABU and T.S. PRASANNA KUMAR

An indigenous, non-linear, and coupled finite element (FE) program has been developed to predict the temperature field and phase evolution during heat treatment of steels. The diffusional transformations during continuous cooling of steels were modeled using Johnson–Mehl–Avrami–Kornogorov equation, and the non-diffusion transformation was modeled using Koistinen–Marburger equation. Cylindrical quench probes made of AISI 4140 steel of 20-mm diameter and 50-mm long were heated to 1123 K (850 °C), quenched in water, and cooled in air. The temperature history during continuous cooling was recorded at the selected interior locations of the quench probes. The probes were then sectioned at the mid plane and resultant microstructures were observed. The process of water quenching and air cooling of AISI 4140 steel probes was simulated with the heat flux boundary condition in the FE program. The heat flux for air cooling process was calculated through the inverse heat conduction method using the cooling curve measured during air cooling of a stainless steel 304L probe as an input. The heat flux for the water quenching process was calculated from a surface heat flux model proposed for quenching simulations. The isothermal transformation start and finish times of different phases were taken from the published TTT data and were also calculated using Kirkaldy model and Li model and used in the FE program. The simulated cooling curves and phases using the published TTT data had a good agreement with the experimentally measured values. The computation results revealed that the use of published TTT data was more reliable in predicting the phase transformation during heat treatment of low alloy steels than the use of the Kirkaldy or Li model.

DOI: 10.1007/s11663-014-0069-0

© The Minerals, Metals & Materials Society and ASM International 2014

I. INTRODUCTION

COMPUTER simulation of the quenching process has emerged as an economical and important tool for predicting the temperature field, microstructure, and mechanical properties of the parts being quenched. The problem of quenching simulation is inter-disciplinary and it involves three distinct fields *viz.* (i) thermal, (ii) mechanical, and (iii) metallurgical fields. The coupling between them during quenching can be found, for example, in References 1, 2, and 10. It becomes inevitable to consider the phase transformation modeling during numerical modeling of heat treatment processes. Finite element (FE) method has extensively been used for quenching simulation in the literature. A number of general purpose FE packages are available to solve multitude of problems involved in engineering, but many problems still remain which prevents their use. Heat treatment processing with phase transformation is

one such a problem. Though, several heat treatment simulation packages are available (*e.g.*, SYSWELD, HEARTS, DEFORM™-HT, and DANTE), some problems cannot be solved satisfactorily with these commercial FE packages.^[3] The main limitations of these softwares are the use of user sub-routines, syntax to be used, incompatibility issues, *etc.*

Huiping *et al.*^[1] simulated the phase transformation and hardness distribution during the end quenching process of P20 steel using the FE method. Kang and Im^[2] predicted the volume fraction of various phases and temperature distribution during quenching of plain-carbon steels based on a FE method which used Johnson–Mehl–Avrami (JMA) equation and latent heat of transformation. Kakhki *et al.*^[3] programmed the phase transformation models in ANSYS using Ansys Parametric Design Language (APDL) capability to simulate the end quench test and quenching of a gear blank in water and oil. A mathematical model was developed by Denis *et al.*^[4] to predict the state of austenite at the end of heating and to predict the distribution of end microstructure and hardness during cooling of steels. The hardenability of steels was determined through numerical simulation of the end quenching process by Homberg.^[5] Thomas *et al.*^[6] estimated the temperature profile of AISI 4140 steel bar during spray cooling with air and water.

K. BABU, Associate Professor, is with the Department of Mechanical Engineering, SSN College of Engineering, Kalavakkam, Chennai 603 110, India. Contact e-mails: babuk@ssn.edu.in; babhu79@gmail.com T.S. PRASANNA KUMAR, Professor, formerly with the IIT Madras, Chennai, India, is now with the Thermet Solutions Pvt. Ltd., Bangalore 560 060, India.

Manuscript submitted November 7, 2013.

Article published online April 19, 2014.

An FE procedure was developed by Woodard *et al.*^[7] to predict the temperature field, microstructure, and hardness distribution during quenching of 1080 steel cylinders and they stressed the importance of accounting the latent heat of phase transformation. Serajzadeh^[8] presented a mathematical model based on FE method and JMA equation to predict the temperature field and microstructures during cooling of steel parts. Kang and Im^[9] predicted the stress–strain distribution in steels using a 3-D thermo-elastic–plastic FE program. Carlone *et al.*^[10] used ANSYS with a user written sub-routine to predict the temperature field, phase evolution, and hardness distribution during quenching of 1080 steel in water. Oliveira *et al.*^[11] employed a multi-phase constitutive model to simulate air cooling and water quenching of steel cylinders using ANSYS. The modeling of diffusional transformations during quenching in majority of the literatures is based on the JMA equation.

Kirkaldy and Venugopalan^[12] proposed a phase transformation model to predict the diffusional transformations during continuous cooling of low alloy steels. Buchmayr and Kirkaldy^[13] developed a computer model based on FE method to simulate the quenching performance of axisymmetric parts by using the Kirkaldy model and also the Johnson–Mehl–Avrami–Komogorov (JMAK) equation in conjunction with the published TTT diagram. Later, the Kirkaldy model was widely used for the simulation of continuous cooling processes of low alloy steels and to predict the microstructures in heat-affected zone (HAZ) during welding. Watt *et al.*^[14] used the Kirkaldy model in a FE-based heat transfer model to predict the microstructure in HAZ during welding. Nguyen and Weckman^[15] also used the Kirkaldy model to calculate the volume fraction of the microstructures and overall hardness distribution in HAZ during the friction welding of AISI 1045 steel. Akerstrom and Oldenburg^[16] used Kirkaldy’s rate equation to predict austenite decomposition in boron steel with modifications to account for austenite stabilization effects resulting from the presence of boron. After 16 years of use, Kirkaldy model was reconstituted by Li *et al.*^[17] to address some of the discrepancies which had been noted in predictions generated by the model.

The results of quenching simulation depend on the accuracy of the boundary condition specified. The heat transfer coefficient of the medium or heat flux values at the part’s surface are regarded as key parameters for numerical simulation of the quenching process. Heat transfer during quenching is very complex and controlled by different cooling mechanisms. Estimation of the unknown thermal boundary condition from the measured temperature data during quenching is based on the Inverse Heat Conduction (IHC) method. Prasanna Kumar^[18] described a serial solution method for a 2-D IHC problem to estimate multiple heat flux components and used it to estimate heat flux components at the metal/mold interface during casting.^[19] The same 2-D serial IHC algorithm was used to compute the surface heat flux by Babu and Prasanna Kumar^[20–22] and a model for the heat flux boundary condition for

quenching simulation was proposed and validated.^[20] The present work, is essentially a validation of the heat flux model developed by the authors^[20] when applied to a low-alloy steel during water quenching. Since quenching simulation requires coupling of both heat transfer and austenite decomposition models, the authors have considered three sources of TTT data and well-accepted models for both diffusion and diffusionless transformations of austenite, as explained below.

The FE program developed in this work uses the JMAK equation for predicting the diffusional phase transformations. The diffusionless transformation is modeled using the Koistinen and Marburger (KM) equation.^[23] The continuous cooling processes of AISI 4140, a low alloy steel, in water and air have been simulated in the FE program with the heat flux boundary conditions. The isothermal transformation start and finish times were taken from the published TTT data of AISI 4140 steel and were also calculated using the Kirkaldy model^[12,27] and the Li model.^[17] Cylindrical quench probes with a diameter of 20 mm and a length of 50 mm were cooled in air, and water and time–temperature data were recorded at the selected interior locations. The heat-treated probes were then sectioned at the mid plane and microstructures were taken. The simulated results were compared with the experimentally measured cooling curves and amount of phases. The results revealed that neither Kirkaldy model nor Li model was reliable in predicting the diffusional phase transformations during continuous cooling of low alloy steels.

II. FINITE ELEMENT MODELING OF HEAT TREATMENT

The FE program has been coded in Visual C++ to simulate the temperature field and phase evolution in 2-D solution domains during heat treatment of steels. According to Fourier law, the governing equation for the heat conduction of transient problems in 2-D Cartesian system having an internal heat source can be written using the energy equilibrium and is given in Eq. [1].

$$k \frac{\partial}{\partial x} \left(\frac{\partial T(x,y,t)}{\partial x} \right) + k \frac{\partial}{\partial y} \left(\frac{\partial T(x,y,t)}{\partial y} \right) + \dot{q} = \rho c \left(\frac{\partial T(x,y,t)}{\partial t} \right) \quad [1]$$

The above equation has to be solved numerically for the unknown temperature with appropriate initial and boundary conditions. The initial condition for quenching and other heat treatment processes is the soaking temperature of the specimen, from which the steels are cooled continuously. The boundary condition required to solve Eq. [1] can be either heat flux or convective boundary and is given in Eqs. [2] and [3], respectively. The heat flux in Eq. [2] and heat transfer coefficient in Eq. [3] can be specified as a constant or as a function of either time or temperature.

$$-k \left(\frac{\partial T}{\partial x} n_x + \frac{\partial T}{\partial x} n_y \right) = q \quad [2]$$

$$-k \left(\frac{\partial T}{\partial x} n_x + \frac{\partial T}{\partial x} n_y \right) = h(T - T_q) \quad [3]$$

After applying the standard Galerkin method of finite element discretization using 3 node triangular elements, the elemental matrix equation takes the form of Eq. [4].

$$[C]\{\dot{T}\} + [K]\{T\} = \{F\} \quad [4]$$

The above first-order differential equation is integrated into time domain using the standard finite difference scheme.^[13] The so-called “ θ ” family of time-domain integration is used and the final matrix equation takes the form of Eq. [5], which can be solved using Gauss–Siedel iterative method.

$$([C] + \theta \Delta t [K])\{T\}^{n+1} = ([C] + (1 - \theta) \Delta t [K])\{T\}^n + \Delta t \left(\theta \{F\}^{n+1} + (1 - \theta) \{F\}^n \right) \quad [5]$$

In Eq. [5], the value of “ θ ” decides the time-marching scheme and different time-marching schemes can be used in the FE program by changing the value of “ θ .” A “ θ ” value of 1 (backward Euler or implicit method) which is unconditionally stable for all the time steps has been used in the FE program. The numerical solution becomes non-linear when the thermo-physical properties of the material and/or the surface heat flux or heat transfer coefficient are specified as a function of temperature. In such cases, the capacitance matrix $[C]$ having specific heat term, the stiffness matrix $[K]$ having the thermal conductivity term, and the force vector $\{F\}$ having boundary condition and heat source terms are to be calculated at future time step $(n + 1)$. These quantities at future time step $(n + 1)$ are calculated iteratively until the temperature difference at each node between successive iterations is less than an acceptable value. A temperature difference of 0.01 K (-273.14 °C) is used as a convergence limit.

A. Phase Transformation Modeling

During continuous cooling of steel parts from their austenitization temperature, the austenite decomposes into several product phases depending on the cooling rate and steel chemistry. The diffusional transformations during austenite decomposition are modeled using the well-known JMAK equation.^[1–3,8–10] According to JMAK model, the volume fraction, X of i^{th} phase in j^{th} time step is given by Eq. [6].

$$X_i^j = 1 - \exp[-b(T_j) t_j^{n(T_j)}], \quad [6]$$

$$\text{where } n(T_j) = \frac{\ln[\ln(1 - X_s)/\ln(1 - X_f)]}{\ln(\tau_s/\tau_f)}$$

$$b(T_j) = -\frac{\ln(1 - X_s)}{t_s^n}$$

The JMAK equation is applicable only for isothermal transformations. For continuous cooling processes like quenching, JMAK equation is to be used in conjunction with the additivity rule. The additivity rule was proposed by Scheil to evaluate the time needed for nucleation and growth of a product phase under continuous cooling conditions.^[10] According to Scheil’s additivity principle, it is assumed that for each time step, j the infinitesimal time, Δt_j spent at temperature, T_j divided by the incubation time at that temperature, $\tau_s(T_j)$ is a fraction of the total incubation time required. As a consequence, the transformation starts, *i.e.*, 1 pct of phase is assumed to form under continuous cooling when Eq. [7] is satisfied.

$$\sum_{j=1}^m \frac{\Delta t_j}{\tau_s(T_j)} \geq 1 \quad [7]$$

Once the incubation is over, the growth of that phase is modeled using the additivity principle as follows. The cooling curve is first sub-divided into a number of infinitesimal time steps (Δt). The amount of phase that transformed isothermally at each time step is calculated using JMAK equation and summed up over the entire time. The procedure of using JMAK equation and Scheil’s additivity principle for the nucleation and growth of a phase is schematically represented by Kang and Im.^[2,9]

According to JMAK equation, for each time step, j corresponding to the temperature, T_j the cumulative volume fraction of i^{th} phase transformed until the previous time step, X_i^{j-1} results in a fictitious time, $t_{j, \text{fict}}$.^[10] The fictitious time, $t_{j, \text{fict}}$ represents the time needed at the current time step to obtain the same amount of cumulative transformed phase at the previous temperature, T_j . The fictitious time, $t_{j, \text{fict}}$ is given by Eq. [8].

$$t_{j, \text{fict}}(T_j) = \left[\frac{-\ln(1 - X_i^{j-1})}{b(T_j)} \right]^{\frac{1}{n(T_j)}} \quad [8]$$

As a result, the current time, t_j at the temperature, T_j can be written as a sum of the current time step, Δt_j and the fictitious time and is given by Eq. [9].

$$t_j = \Delta t_j + \left[\frac{-\ln(1 - X_i^{j-1})}{b(T_j)} \right]^{\frac{1}{n(T_j)}} \quad [9]$$

The amount of phase transformed at the current time step is then calculated by substituting Eq. [9] in Eq. [6]. The concept of using a fictitious time step is illustrated by Carlone *et al.*^[10] The difference between the amount of phases transformed till the current time step, t_j and the previous time step, t_{j-1} would give the fraction of phase transformed during the current time step, Δt_j . This transformed fraction of phase is used to calculate the

latent heat of phase transformation in the current time step. The various phases are assumed to transform only within their corresponding transformation start and finish temperatures. The volume fraction of martensite transformed, X_m is calculated using KM equation and is given by Eq. [10].

$$X_m = 1 - \exp[-0.011(M_s - T)] \quad [10]$$

B. Austenite Decomposition Model by Kirkaldy *et al.*

The isothermal transformation kinetics of diffusional transformations during continuous cooling of low alloy steels was modeled by Kirkaldy and Venugopalan.^[12] The development of Kirkaldy model was based on the thermodynamics and kinetic principles of solid–solid phase transformations. The general form of their reaction kinetics of austenite decomposition is described by Zener and Hillert type formula and is given by Eq. [11].

$$\tau(X, T) = \frac{F(C, Mn, Si, Ni, Cr, Mo, G)}{\Delta T^{n1} \exp[-Q/R(T + 273)]} I(X), \quad [11]$$

$$\begin{aligned} \text{where } \frac{1}{D} &= \frac{1}{\exp(-27, 500/RT)} + \frac{0.01Cr + 0.52Mo}{\exp(-37, 500/RT)} \\ \tau_B &= \frac{(2.34 + 10.1C + 3.8Cr + 19Mo)10^{-4}}{2^{(G-1)/2}(B_s - T)^2 \exp(-27, 500/RT)} \\ &\quad \times \int_0^X \frac{\exp(AX^2)}{X^{2(1-X)/3}(1-X)^{2X/3}}, \end{aligned} \quad [14]$$

where $A = (1.9C + 2.5Mn + 0.9Ni + 1.7Cr + 4Mo - 2.6)$

C. Austenite Decomposition Model by Li *et al.*

The Kirkaldy rate equations were modified by Li *et al.*^[17] to address some of the discrepancies. The Li model for isothermal transformation time of ferrite, pearlite, and bainite is given by Eqs. [15], [16], and [17]. The major differences between the Li model and Kirkaldy model lie in the effect of steel composition, grain size effect, and the reaction rate term, the details of which can be found in.^[17]

$$\tau_F = \frac{\exp(1.00 + 6.31C + 1.78Mn + 0.31Si + 1.12Ni + 2.70Cr + 4.06Mo)}{2^{0.41G}(A_{e3} - T)^3 \exp(-23, 500/RT)} I(X) \quad [15]$$

$$\tau_P = \frac{\exp(-4.25 + 4.12C + 4.36Mn + 0.44Si + 1.71Ni + 3.33Cr + 5.19\sqrt{Mo})}{2^{0.32G}(A_{e1} - T)^3 \exp(-27, 500/RT)} I(X) \quad [16]$$

$$\tau_B = \frac{\exp(-10.23 + 10.18C + 0.85Mn + 0.55Ni + 0.90Cr + 0.36Mo)}{2^{0.29G}(B_s - T)^2 \exp(-27, 500/RT)} I(X), \quad [17]$$

where “ F ” is a function of steel’s chemical composition in wt pct and prior austenite grain size, G in ASTM number. Essentially, the Kirkaldy model consists of Eqs. [12], [13], and [14] which describe the isothermal transformation time of ferrite, pearlite, and bainite, respectively.

$$\begin{aligned} \tau_F &= \frac{59.6Mn + 1.45Ni + 67.7Cr + 244Mo}{2^{(G-1)/2}(A_{e3} - T)^3 \exp(-23, 500/RT)} \\ &\quad \times \int_0^X \frac{dX}{X^{2(1-X)/3}(1-X)^{2X/3}} \end{aligned} \quad [12]$$

$$\begin{aligned} \tau_P &= \frac{1.79 + 5.42(Cr + Mo + 4Mo.Ni)}{2^{(G-1)/2}(A_{e1} - T)^3 D} \\ &\quad \times \int_0^X \frac{dX}{X^{2(1-X)/3}(1-X)^{2X/3}}, \end{aligned} \quad [13]$$

$$\text{where } I(X) = \int_0^X \frac{dX}{X^{0.4(1-X)}(1-X)^{0.4X}}$$

In the Kirkaldy model and the Li model, the temperature, T is in K and volume fraction, X is the normalized volume fraction which is defined as the ratio of the true fraction to the equilibrium fraction of each phase.

D. Critical Transformation Temperatures

The A_{e3} temperature can be calculated based on the thermodynamic models using an ortho-equilibrium approach, which assumes full partitioning of the alloying elements. However, considering the difficulties of the thermodynamic model, the empirical expression proposed by Kirkaldy and Barganis as found in^[24] is used for calculating the A_{e3} temperature and is given by Eq. [18]. Similarly, A_{cm} temperature is calculated using an empirical equation proposed by Lusk *et al.* as found

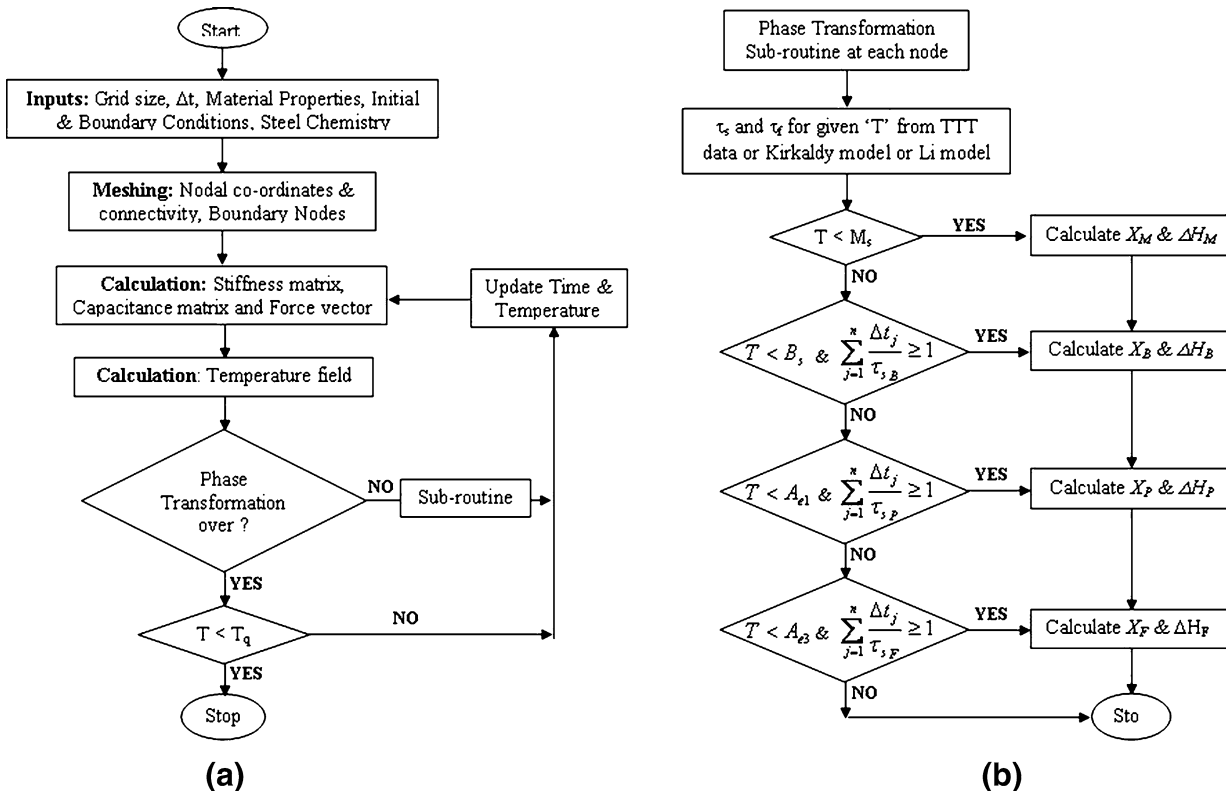


Fig. 1—Flow chart of (a) non-linear, coupled FE program, (b) phase transformation calculation in FE program.

in^[24] and is given in Eq. [19]. Similar types of expressions for A_{e3} and A_{cm} temperatures were used by Watt *et al.*^[14] and Nguyen and Weckman^[15] in their work.

$$A_{e3} = 912 - 203C^{0.5} + 15.2Ni + 44.7Si + 31.5Mo - 30Mn - 11Cr \quad [18]$$

$$A_{cm} = 217.5 + 977.65C - 417.57C^2 - 35.29Cr + 21.36C Cr - 1.5Cr^2 - 0.95Mn - 1.37C Mn - 2.76Mo - 3.77C Ni + 30.36Si - 8.10C Si + 2.58Cr Si \quad [19]$$

Kirkaldy and Venugopalan^[12] used an expression for bainite start temperature which was independent of austenite grain size and the same as given by Eq. [20] is followed in the FE program. Kung and Rayment^[25]

tion of M_s temperature as given by Eq. [21] is followed in this work.

$$B_s = 637 - 58C - 35Mn - 15Ni - 34Cr - 41Mo \quad [20]$$

$$M_s = 539 - 423C - 30.4Mn - 12.1Cr - 17.7Ni - 7.5Mo - 7.5Si \quad [21]$$

E. Austenite Grain Growth Model

The austenite grain size term in Kirkaldy model and Li model was calculated using the model proposed by Lee and Lee^[26] for low alloy steels. The model was based on Arrhenius type equation and was obtained by fitting the measured austenite grain size data as a function of alloying elements, temperature, and time and is given by Eq. [22].

$$G \text{ (in } \mu\text{)} = 76,671 \exp\left(-\frac{89,098 + 3581C + 1211Ni + 1443Cr + 4031Mo}{RT}\right) t^{0.211} \quad [22]$$

reviewed a number of empirical formulae for M_s temperatures and stated that M_s temperature predicted by Andrew's formula was close to the experimentally measured values. The Andrew's formula for the predic-

A non-linear regression equation as given by Eq. [23] was used to convert the austenite grain size in mm into its equivalent ASTM grain size number as used in the work of Nguyen and Weckman.^[15]

$$G \text{ (ASTM Number)} = -2.89 * \log(G \text{ in mm}) - 2.95 \quad [23]$$

$$\Delta H_F = (1769 - 5.725T + 0.0062T^2 - 2.303 \times 10^{-6}T^3) \times 10^6 \quad [25]$$

$$\Delta H_{P \text{ or } B} = 1.560E^9 - 1.500E^6 T \quad [26]$$

$$\Delta H_M = 6.40E^8 \quad [27]$$

F. Latent Heat of Phase Transformation

The latent heat evolved due to solid–solid phase transformation during continuous cooling of steel in each element of the FE program was regarded as a source of internal heat generation and the heat generation rate is modeled using Eq. [24]. The enthalpy of ferrite transformation was calculated by using Eq. [25] as used in the work of.^[2,3,9] The enthalpy of pearlite/bainite and martensite transformation is given by Eqs. [26] and [27] as used by Oliveira *et al.*^[11] The flow chart of the non-linear FE program coupled with phase transformation calculations is given in Figures 1(a) and (b).

$$\dot{q} = \frac{\Delta X_i}{\Delta t} \Delta H_i \quad [24]$$

G. Benchmarking of FE Program

The FE program developed for this work was validated by taking two benchmark problems of continuous cooling processes. One with an arbitrarily chosen transient heat flux of parabolic nature as shown in Figure 2(a) and another one with the temperature-dependent heat flux during quenching as shown in Figure 2(b), the results of FE simulation were validated. The temperature-dependent heat flux in Figure 2(b) was calculated from the surface heat flux model proposed by

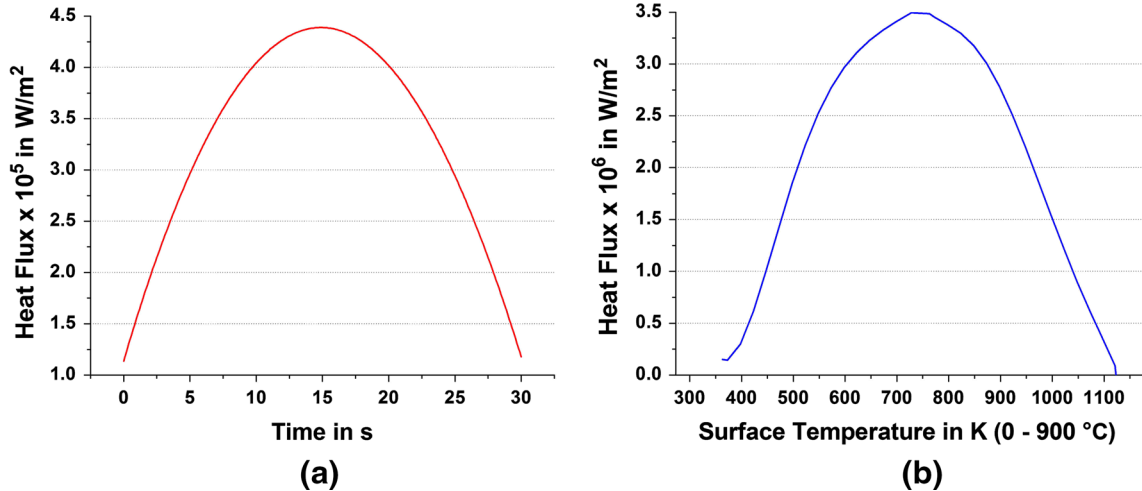


Fig. 2—(a) Parabolic and (b) quenching heat flux used for benchmarking the FE program.

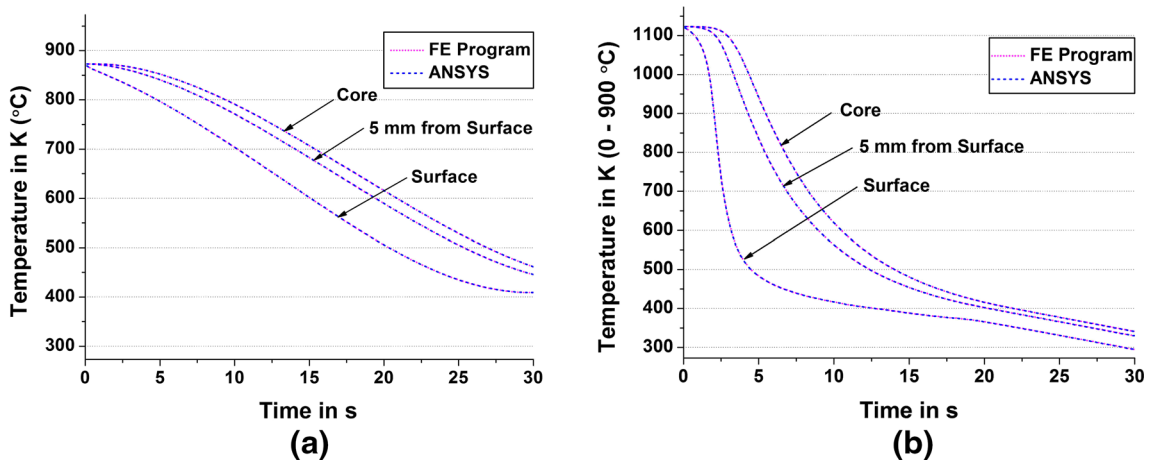


Fig. 3—Cooling curves predicted by FE program and ANSYS for (a) parabolic and (b) quenching heat flux boundaries.

the authors in Reference 20 for a soaking temperature of 1123 K (850 °C). One quadrant of a circle with a radius of 10 mm was chosen as a solution domain in the FE program and was discretized into 1089 elements of 3 node triangular elements as described in Reference 20. The same solution domain was modeled and discretized in a commercial FE package, ANSYS but with 6 node triangular elements (Element No. 35). The cylindrical surface was assigned with parabolic and quenching heat fluxes as boundary conditions and the cooling processes were simulated at 873 K and 1123 K (600 °C and 850 °C), respectively, in both the FE program and ANSYS.

The two cooling processes were simulated with a time step of 0.1 second for 30 seconds using the temperature-dependent material properties of SS 304L taken from Reference 20. The thermal responses retrieved from ANSYS and the FE program at the core, 5 mm from surface and surface are compared in Figures 3(a) and (b) for the input heat flux of parabolic and quenching nature, respectively. The almost exact agreement sug-

gests that the non-linear FE program developed in this work is functionally equivalent to ANSYS for the two benchmarking problems.

In Figures 3(a) and (b), the simulated cooling curves at different locations in ANSYS and the FE program are not distinguishable. Hence, the percentage errors between the cooling curves simulated in ANSYS and the FE program at different locations were calculated and plotted as a function of temperature in Figures 4(a) and (b) for the parabolic and quenching heat flux boundary conditions, respectively. The maximum error is -0.138 pct at 442 K (169 °C) and 0.65 pct at 323 K (50 °C) for the parabolic and quenching heat flux boundaries, respectively.

The sub-routines meant for calculating the isothermal transformation start and finish times in the FE program using the Kirkaldy model and the Li model have been validated as follows. The TTT diagram of AISI 4140 steel was calculated using the Kirkaldy model by the sub-routine with the exact inputs as used by Buchmayr and Kirkaldy.^[13] This calculation is compared with their predicted curves and also with the published TTT diagram in Figure 5(a).

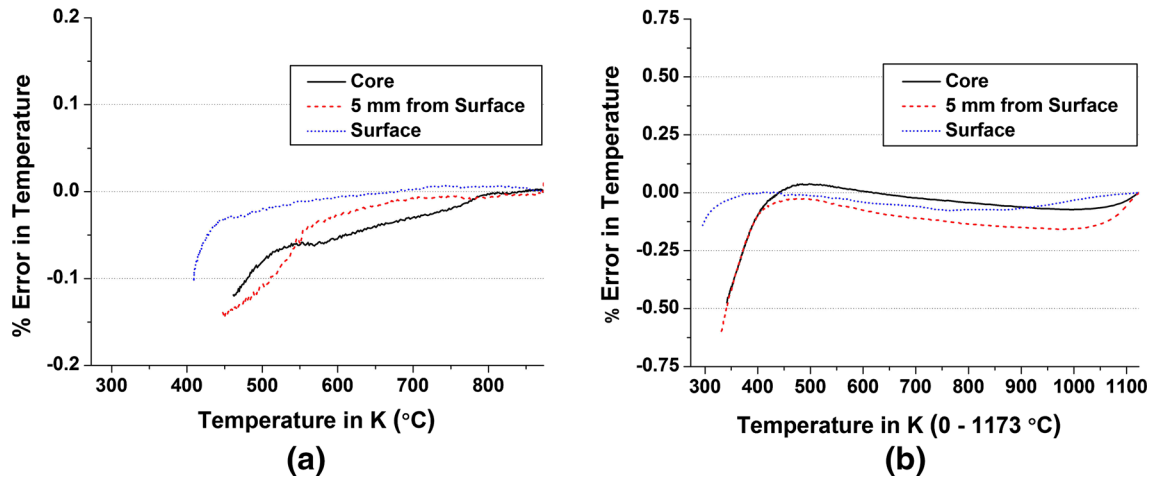


Fig. 4—Percentage errors in cooling curves predicted by ANSYS and FE Program for (a) parabolic and (b) quenching heat fluxes.

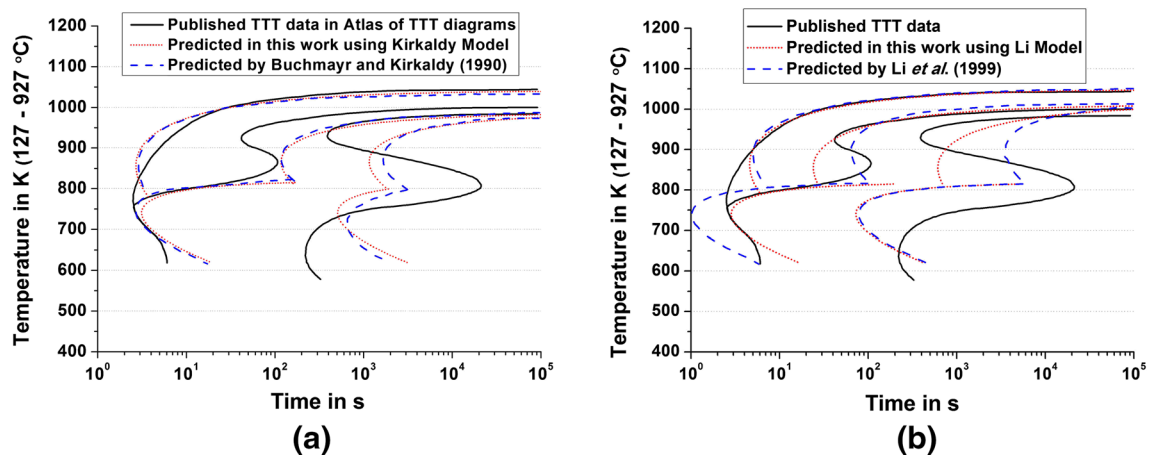


Fig. 5—Comparison of predicted TTT diagram using (a) Kirkaldy model, (b) Li model by FE program with the literature values and published TTT data.

Table I. Chemical Composition of AISI 4140 Steel

Element	C	Mn	Cr	Si	Mo	Ni
wt pct	0.39	0.55	1.03	0.28	0.18	0.08

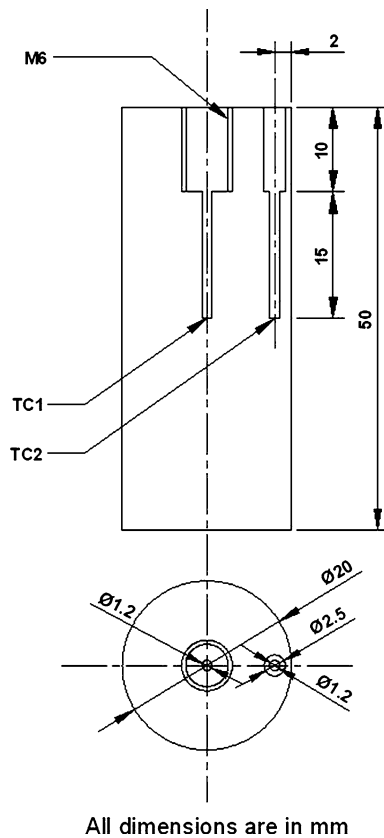


Fig. 6—Schematic of the quench probe (all dimensions are in mm).

The predicted values agree well with the predictions published by Buchmayr and Kirkaldy.^[13] However, the predicted values in this work as well by Buchmayr and Kirkaldy^[13] have significant deviations with the published TTT data. Similarly, the predicted TTT diagram using Li model by the sub-routine for the exact input values as found in^[17] is compared with the predicted values by Li *et al.*^[17] and with published TTT diagram in Figure 5(b). The predicted values in this work have big differences from the predicted TTT published by Li *et al.*^[17]. The sub-routine has been thoroughly rechecked as per the Li model published in Reference 17. Another point to be noted here is that the TTT data originally predicted by Li *et al.*^[17] itself have big deviations from the published TTT data and the reason for these disagreement is unclear.

III. EXPERIMENTAL PROCEDURE

Cylindrical quench probes with a diameter of 20 mm and a length of 50 mm were machined from a steel rod having a nominal alloy composition of AISI 4140. The chemical composition of the selected steel rod of AISI 4140 steel was measured at the National Metallurgical

Laboratory, Chennai, India using Optical Emission Spectrometry and is given in Table I. The schematic of the quenching probes used is shown in Figure 6. The design is the same as the one used in References 20 through 22. The quench probes were turned and faced in a central lathe machine (HMT—Type LB/17, No. 9970, Bangalore, India) whose least count is 0.05 mm. At the top end of the probe, an M6 thread was cut for 10-mm depth along the axis to which a long connecting stem was attached. The purpose of using a stem was to assist with handling the specimen between the heating furnace and quench tank. A hole of 1.2-mm diameter was drilled along the axis for a depth of 15 mm below the threaded portion in order to fix the first thermocouple TC1. Another hole of same diameter with its axis 2 mm below the cylindrical surface was drilled for 25-mm depth to fix the second thermocouple TC2. The top end of this hole was bored to 2.0-mm diameter for a depth of 10 mm so as to facilitate the use of an adhesive paste to fix TC2 securely in its position. The holes for fixing TC1 and TC2 were drilled in the quench probes using a high precision vertical milling machine (MAN-FORD—Model No. 5 kV, Taichung Hsien, Taiwan) instead of drilling in a regular drilling machine. In vertical milling machine, the x, y, and z movements were digitized to an accuracy of 0.0001 mm. The axis of the holes was precisely located and drilled with a very low feed, but at a high spindle speed.

Two mineral insulated K-type thermocouples of 1 mm sheath wire diameter were used for temperature measurements. One of the thermocouples was calibrated in a muffle furnace in the temperature range from 323 K to 873 K (50 °C to 600 °C). The calibration result of the thermocouple showed a maximum percentage deviation of 0.34 pct at 873 K (600 °C). Time–temperature data were recorded using a data-acquisition system (Agilent—Model No. 34970A, Loveland, CO) during the continuous cooling processes. The probe was heated in a vertical electric resistance tubular furnace to 1123 K (850 °C), soaked for 10 minutes, and then quenched in still water maintained at 303 K (30 °C). Another quench probe was cooled from 1123 K (850 °C) after soaking for 10 minutes in air at 301 K (28 °C). The water-quenched and air-cooled probes were sectioned at the mid plane, mechanically polished and etched with 2 pct Nital. The etched surfaces were characterized under microscopes for microstructures. The microstructures were taken at the core and surface of the probe section using an optical microscope (OM) and scanning electron microscope (SEM) (FEI Quanta 200, Oregon, US).

A. Experimental Results and Microstructure Analysis

The temperature data measured during water quenching and air cooling of the quench probes at TC1 and TC2 locations are plotted in Figures 7(a) and (b), respectively. The temperature recorded at TC1 and

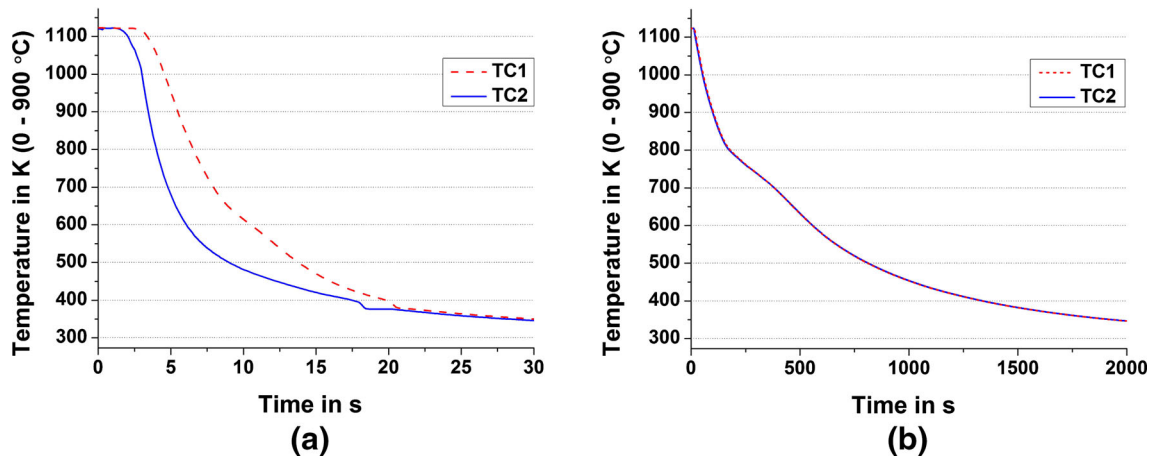


Fig. 7—Measured cooling curve during cooling of 4140 steel in (a) water, (b) air.

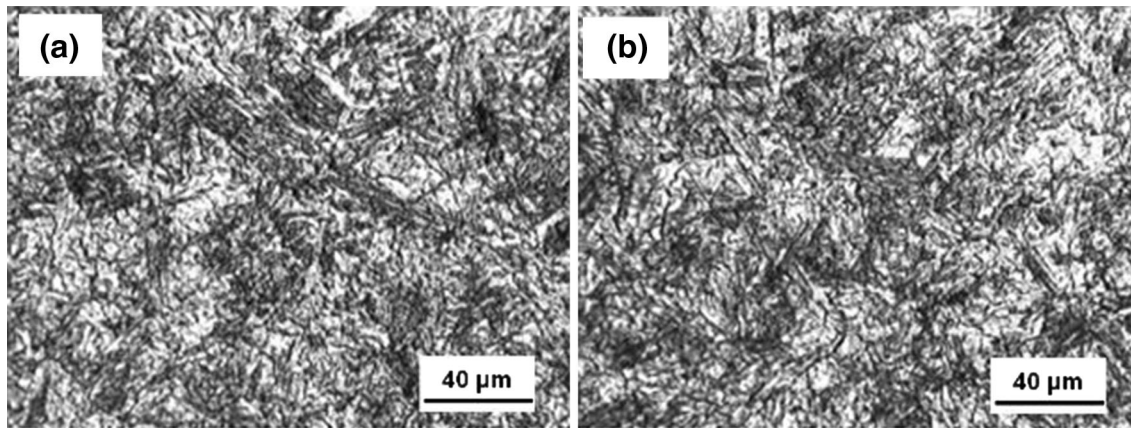


Fig. 8—OM picture of water-quenched probe at (a) surface, (b) core.

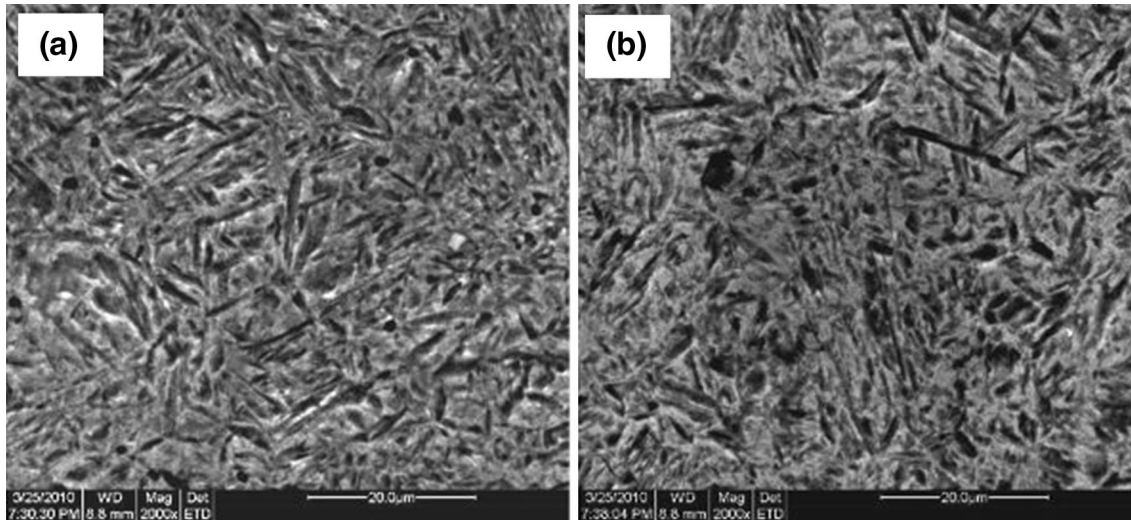


Fig. 9—SEM picture of water-quenched probe at (a) surface, (b) core.

TC2 locations during air cooling is hardly distinguishable except during the start of the process, since the cooling rate was very slow and there is no temperature gradient inside the probe.

The microstructures of the water-quenched AISI 4140 steel taken by OM and SEM are shown in Figures 8 and 9, respectively. The microstructure taken by OM was analyzed for the amount of various phases using

QUANTIMET, the image analysis software. The microstructures invariably consist of lath martensite across the probe section with a very little retained austenite. The small amount of retained austenite was not accurately traceable and thus the water-quenched probe was assumed to consist of 100 pct martensite. The microhardness measurements taken at ten different locations across the water-quenched probe section with 0.2 kg load showed a variation from 633 to 669 HV with an average of 647 HV. This hardness corresponds to a typical martensite hardness value.

The microstructures of the air-cooled AISI 4140 steel taken by OM and SEM are shown in Figures 10 and 11, respectively. The microstructures across the probe section consist of ferrite and bainite. The SEM pictures clearly show the presence of feathery bainite. The slope of the cooling curves measured during air cooling has a clear inflection at ~ 813 K (540 °C) in Figure 7(b) which is just below the bainite start temperature of the selected steel. The slope of the cooling curves once again changes at ~ 673 K (400 °C) which represents the completion of bainite transformation during air cooling. The measured volume fraction of ferrite and bainite from the optical

microstructures using QUANTIMET is 32 and 68 pct, respectively. The microhardness values taken at ten different locations across the air-cooled probe section varied from 348 to 366 HV, and the average microhardness was 357 HV.

IV. FINITE ELEMENT SIMULATION OF STEEL HEAT TREATMENT

The continuous cooling processes of AISI 4140 steel in water and air were simulated with the temperature-dependent heat flux values as boundary conditions in the FE program. The simulated results of water quenching and air cooling of AISI 4140 steel were validated by comparing them against the experimentally measured values.

A. Finite Element Model

A single unknown heat flux boundary is assumed along the probe/quenchant interface. The mid section of the quench probe, where thermocouple tips were

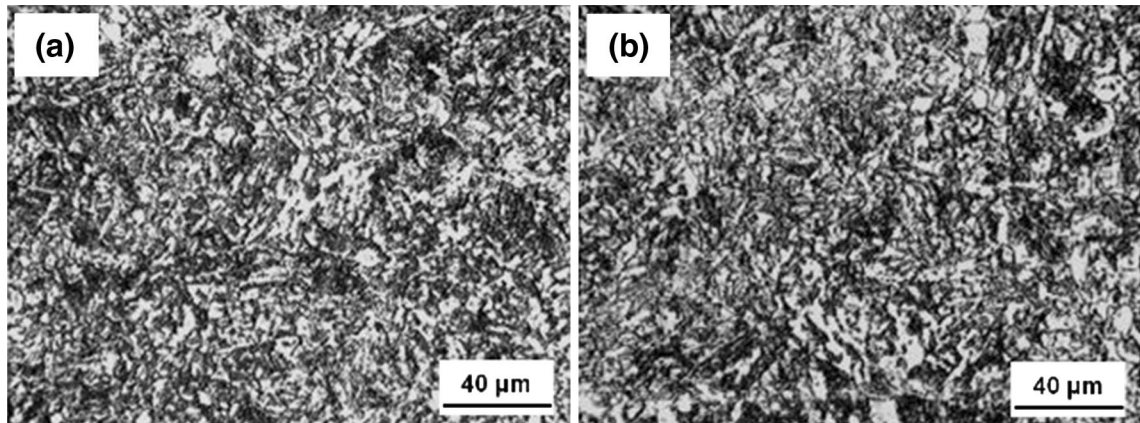


Fig. 10—OM picture of air-cooled probe at (a) surface, (b) core.

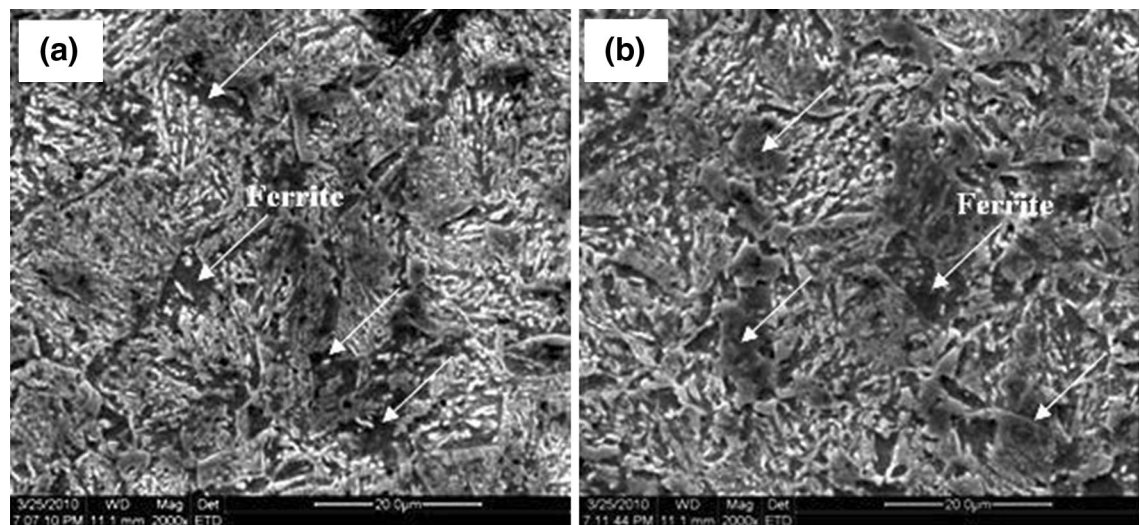


Fig. 11—SEM picture of air-cooled probe at (a) surface, (b) core.

positioned, was taken as the model domain neglecting the end effects for the estimation of unknown heat flux at the quench surface. Due to its circular geometry, one quarter of the solution domain was modeled and discretized using a mesh of 1089 elements (3 node triangular) and the total number of nodes being 595. The FE mesh is shown in Figure 12 in which the surface along x and y axes was assigned zero heat flux as boundary condition and the cylindrical surface was assigned as heat flux boundary condition. The effect of grid size and time step on the simulation results was studied in^[20] for a similar quenching problem.

B. Inputs for FE Simulation of Water Quenching and Air Cooling

The chemical composition of AISI 4140 steel (Table 1) was used in the Kirkaldy model and Li model during the

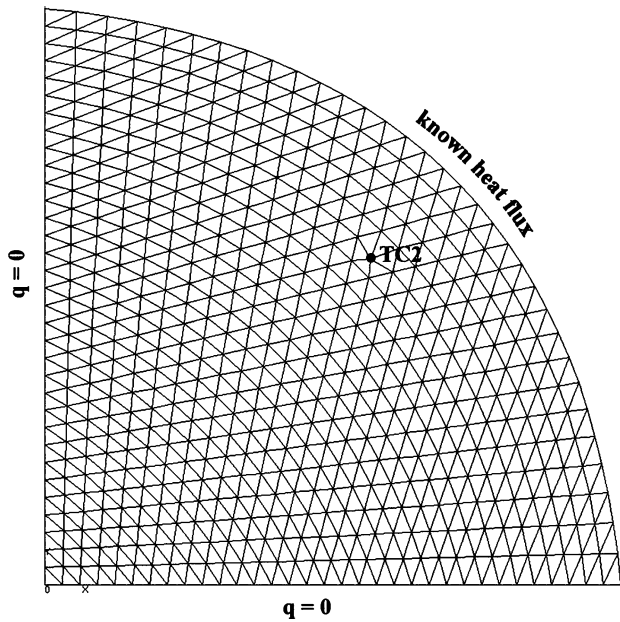


Fig. 12—FE model used for heat treatment simulation.

phase transformation calculations. Temperature- and phase-dependent thermo-physical properties of AISI 4140 as used in Reference 3 were used in the FE simulation of water quenching and air cooling of AISI 4140 steel. A mixture rule was used for calculating the temperature- and phase-dependent thermal conductivity and specific heats and is given in Eqs. [28] and [29], respectively.

$$k = \sum_{i=A,F,P,B,M} X_i k_i \quad [28]$$

$$c = \sum_{i=A,F,P,B,M} X_i c_i \quad [29]$$

The temperature-dependent heat flux shown in Figure 2(b) was used as a boundary condition for the simulation of water quenching of AISI 4140 steel. The heat flux boundary for air cooling simulation was calculated using the IHC method as in Reference 20. For this purpose, a quench probe of same design as shown in Figure 6 was machined from SS 304L and cooled in air from 1123 K (850 °C) after soaking for 30 minutes. The measured cooling curve during air cooling of SS 304L probe at TC2 is shown in Figure 13(a). The estimated heat flux through the IHC method using Figure 13(a) as input is shown in Figure 13(b) and was specified as a boundary condition for the simulation of air cooling of AISI 4140 steel.

C. Calculation of Equilibrium Ferrite

The equilibrium fraction of ferrite, pearlite, and bainite required in the phase transformation calculation by the JMA equation and in the Kirkaldy and Li models was calculated as described in the following. The intersection of A_{e3} and A_{cm} line is the eutectoid temperature (A_{e1}). The equilibrium fraction of ferrite was calculated by applying the Lever rule and the procedure is depicted in Figure 14(a). The equilibrium fraction of ferrite, X_F^{eqb} for AISI 4140 steel was calculated by the FE program using the chemical composition given in Table I. Between A_{e1} and

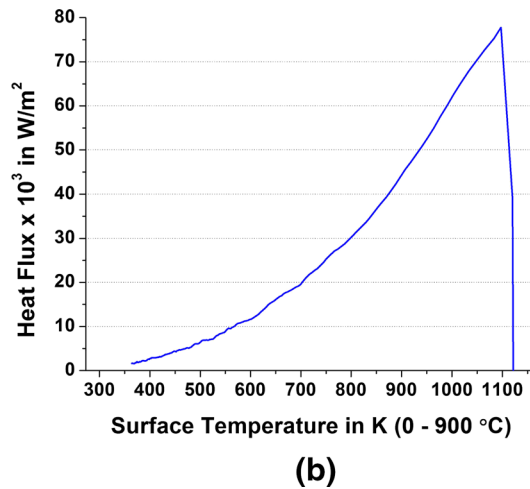
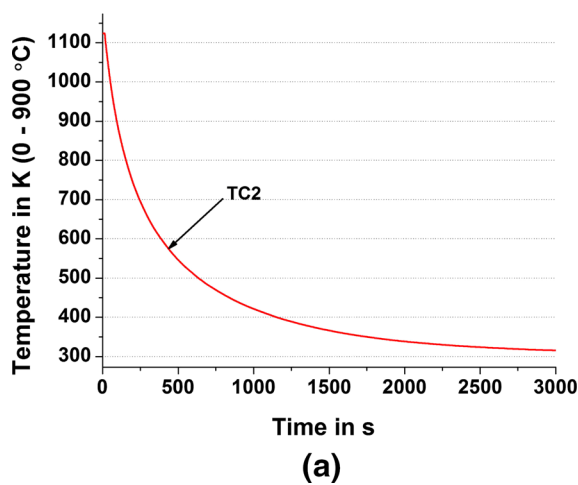


Fig. 13—(a) Measured cooling curve at TC2. (b) Estimated surface heat flux during air cooling of SS 304L probe.

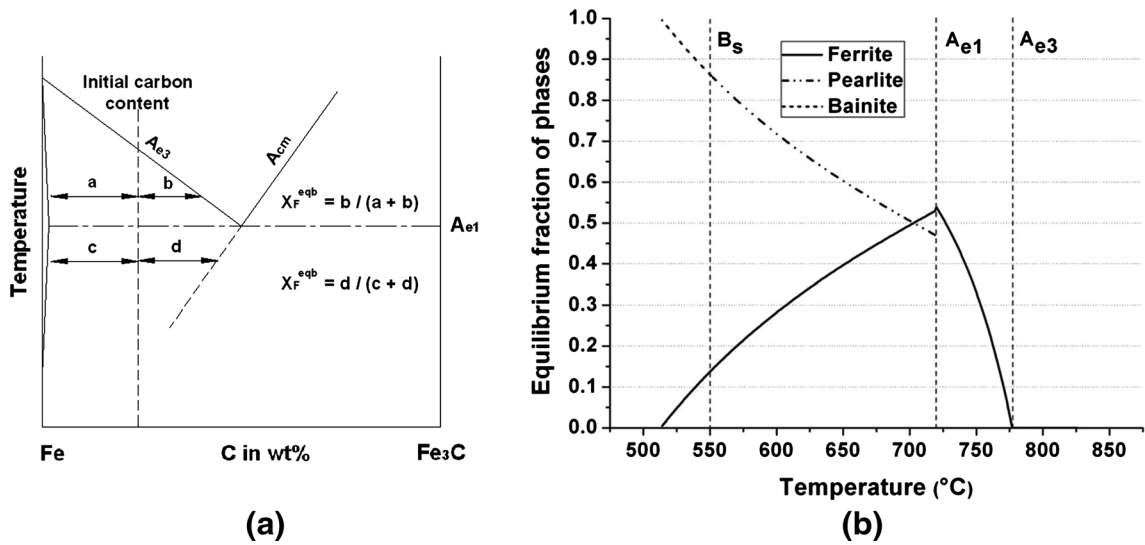


Fig. 14—(a) Illustration of phase diagram and Lever rule. (b) Equilibrium fraction of ferrite, pearlite, and bainite calculated for AISI 4140 steel.

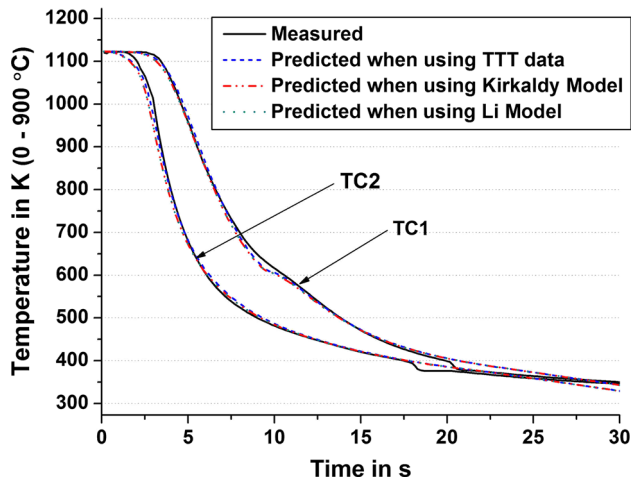


Fig. 15—Measured and simulated cooling curves during water quenching.

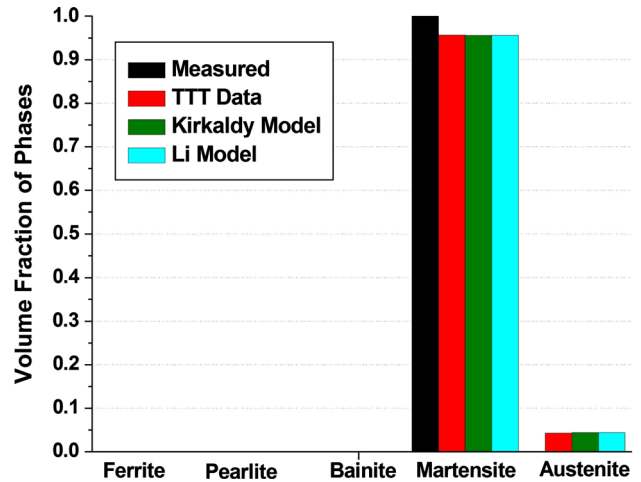


Fig. 16—Measured and predicted phases during water quenching of AISI 4140 steel.

B_s , the equilibrium fraction of pearlite was taken as one minus equilibrium fraction of ferrite. Similarly, between B_s and B_{Nose} , the equilibrium fraction of bainite was taken as one minus equilibrium fraction of ferrite. The calculated amount of equilibrium fraction of ferrite, pearlite, and bainite for AISI 4140 steel is plotted in Figure 14(b).

D. Results of Water Quenching Simulation

Water quenching of AISI 4140 steel was simulated in the FE program with a time step of 0.1 second for 30 seconds. The isothermal transformation time of start and finish of each phase was calculated using Kirkaldy model and Li model in the FE program. Apart from using these models, the published TTT diagram of AISI 4140 steel was digitized and given as input to the FE program. The digitized start and finish “C” curves of ferrite, pearlite, and bainite were treated as step-wise linear in the FE program. Thus, the simulation of water quenching of AISI 4140 steel

probe was carried out using the published TTT data, the Kirkaldy model, and the Li model for the prediction of phase transformation using the JMAK equation. The predicted time-temperature at TC1 and TC2 when using the Kirkaldy model, Li model, and published TTT data is compared with the measured values in Figure 15.

The predicted cooling curves at these locations by all the three methods agree well with the measured values. The time-temperature data predicted by using Kirkaldy model, Li model, and published TTT data are not distinguishable. This good agreement is expected given that only martensite has formed during water quenching and the Kirkaldy model, Li model, and TTT data are meant for predicting the diffusional transformations in conjunction with the JMAK equation. The predicted and measured volume fraction of various phases during water quenching of AISI 4140 steel by using Kirkaldy model, Li model, and published TTT data is compared in Figure 16. The predicted volume fractions of mar-

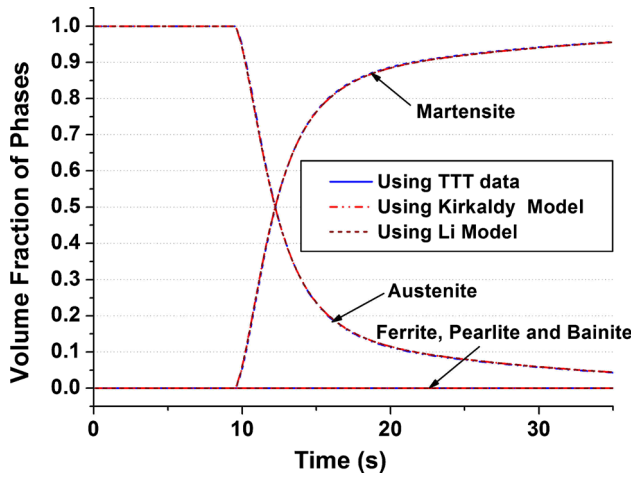


Fig. 17—Evolution of various phases as predicted by FE simulation.

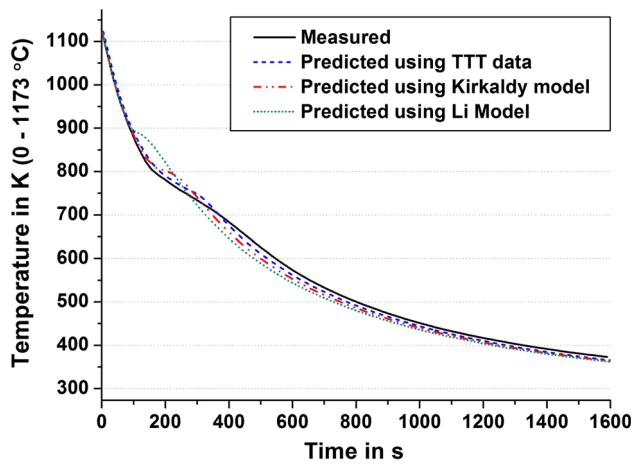


Fig. 18—Measured and predicted time-temperature data at TC2 during air cooling.

tensite and retained austenite by using these different methods were 0.956 and ~ 0.044 , respectively, with a small variation at the third digit after the decimal point. The evolution of martensite and other phases as a function of time as predicted by these different methods during the FE simulation of water quenching of AISI 4140 steel probe is plotted in Figure 17. Again here, the predicted phase evolutions when using Kirkaldy model, Li model, and published TTT data are not distinguishable, since only KM equation was used for the prediction of martensite irrespective of using Kirkaldy model or Li model or published TTT data.

E. Results of Air Cooling Simulation

The process of air cooling was simulated in the FE program for 1600 seconds with a time step of 1.0 second. The predicted time-temperatures at TC2 location when using TTT data, Kirkaldy model, and Li model for phase transformation calculations are compared with the measured values in Figure 18. The predicted cooling curve when using TTT data along with JMAK equation closely follows the measured cooling curve in

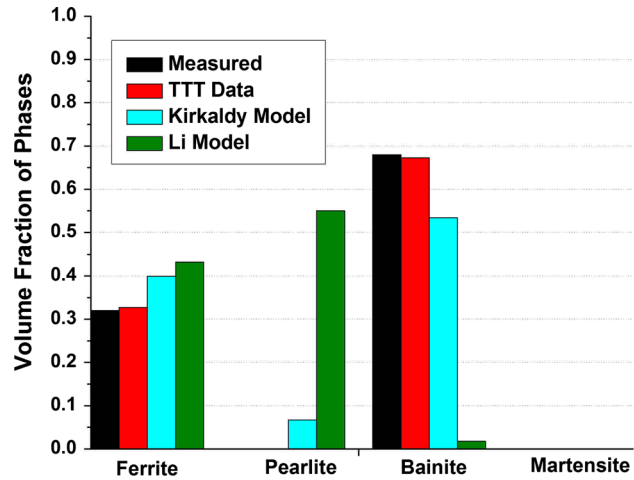


Fig. 19—Measured and predicted phase fractions transformed during air cooling.

Figure 18. The cooling curve predicted when using Kirkaldy model deviates significantly from ~ 793 K (520 °C), which is in the bainitic region of the chosen steel. Similarly, the cooling curve predicted when using Li model deviates significantly from ~ 883 K (610 °C), which is well above the bainite region but below the pearlite start temperature of the chosen steel. The measured and predicted amounts of various phases transformed when using TTT data, Kirkaldy model, and Li model are presented as a bar chart in Figure 19.

The predicted phase fractions when using the published TTT data are very close to the measured values. The use of Kirkaldy model predicted a higher amount of ferrite consequently a lower amount of bainite than the measured amount of ferrite and bainite. Similarly, the use of Li model also predicted a higher amount of ferrite than the measured amount and consequently very high amount of pearlite which is not seen in the air-cooled microstructures. The evolution of various phases with respect to time during air cooling of AISI 4140 steel when using TTT data, Kirkaldy model, and Li model is plotted in Figures 20(a), (b), and (c). The differences in the cooling curves and phase fractions predicted by the Kirkaldy and Li models are explained by the predicted TTT diagrams generated using these models.

Incorrect TTT data used during FE simulation of heat treatment of steels would directly affect the prediction of temperature field, since it affects the latent heat of phase transformation. The predicted TTT diagrams using the Kirkaldy and Li models for the chemical composition of AISI 4140 steel as given in Table I during FE simulation are compared with the published TTT diagram in Figure 21.

The differences in ferrite start “C” curve predicted by the Kirkaldy model from the published one does not have a significant effect on the outcome of the prediction. On the other hand, the difference in the pearlite start “C” curve is significant (please note the logarithmic time scale) and this causes the JMAK equation to overestimate the amount of ferrite when using the Kirkaldy model. Similarly, the large differences in the bainite finish “C” curve predicted using the Kirkaldy model from the published TTT data cause JMAK equation to overestimate the amount of bainite at

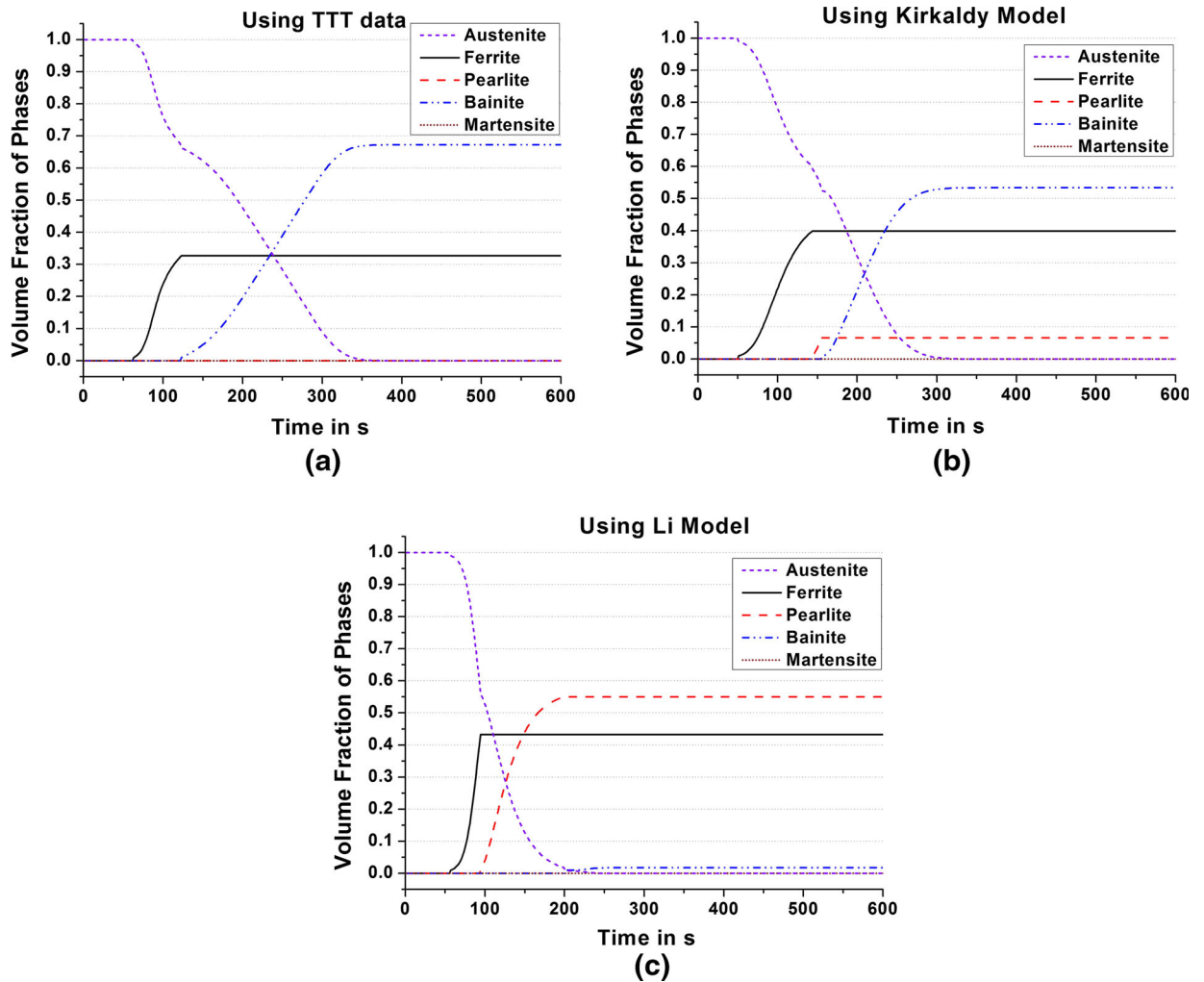


Fig. 20—Evolution of various phases as predicted during air cooling when using (a) published TTT data, (b) Kirkaldy model, (c) Li model.

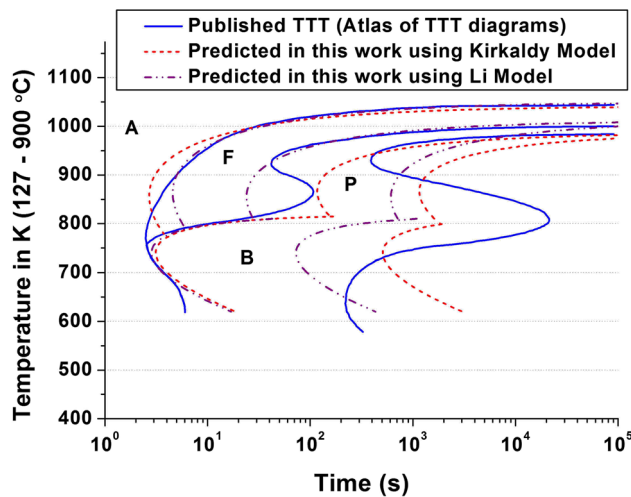


Fig. 21—Comparison of estimated TTT diagram using Kirkaldy model and Li mode with the published TTT diagram for AISI 4140 steel.

the initial stages. It can be further confirmed by comparing the bainite evolution in Figures 20(a) and (b). Thus, the slope of the cooling curve predicted when using Kirkaldy model slows down from 993 K (520 °C) in Figure 18 due to the addition of higher latent heat of bainite transformation. Similarly, the large difference in the pearlite start and finish “C” curves predicted by the Li model from the published one causes a significant impact, by causing JMAK equation to overestimate the amount of ferrite and pearlite. Thus, the slope of the cooling curve predicted when using the Li model decreases below a temperature of 883 K (610 °C) in Figure 18 due to the addition of the latent heat of pearlite transformation

V. CONCLUSIONS

An FE program has been developed and used to simulate the heat treatment of AISI 4140 steel. The use of published TTT data was found to be more reliable in

predicting the diffusional transformations during heat treatment of low alloy steels than the use of either the Kirkaldy or Li models. The differences between the predicted time–temperature and phases using the models and the measured values are due to the difference in the models’ predicted TTT curves and the published TTT data. The simulation of water quenching which created a fully martensitic structure required only the K–M equation for the phase transformation prediction and as a result the simulation results are closely matching with experimentally measured values. The accuracy of the proposed heat flux model for quenching simulation in Reference 20 was further substantiated from the simulation results of the water quenching of AISI 4140 steel in this work.

NOMENCLATURE

A_{e1}	Pearlite transformation start temperature in K (°C)
A_{e3}	Ferrite transformation start temperature in K (°C)
b	Constant of JMAK equation
B_s	Bainite transformation start temperature in K (°C)
c	Specific heat (J/kg K)
G	Austenite grain size (ASTM No.)
h	Heat transfer coefficient (W/m ² K)
I	Reaction term (Integral part) in Kirkaldy model and Li model
k	Thermal conductivity (W/m K)
M_s	Martensite transformation start temperature in K (°C)
n	Exponent of JMAK equation
n_x, n_y	Direction cosines of the outward normal vector
Q	Activation energy for diffusion reaction, (cal/mol)
q	Heat flux (W/m ²)
R	Universal gas constant (cal/K mol)
T	Temperature, in K (°C)
t	Time (s)
X	Volume fraction of phases
ρ	Density (kg/m ³)
\dot{q}	Rate of heat generation (W/m ³)
$[C]$	Capacitance matrix
$[K]$	Element stiffness matrix
$\{\dot{T}\}$	First derivative of the temperature, T
$\{F\}$	Force vector
ΔH	Enthalpy of phase transformation (J/m ³)
ΔT	Degree of undercooling, in K (°C)
Δt	Time step (s)
ΔX	Fraction of phase transformed over Δt
τ	Isothermal transformation time, (s)

SUPERSCRIPIT/SUBSCRIPTS

A Austenite

B Bainite
 eqb Equilibrium
 F Ferrite
 f Finish of transformation
 M Martensite
 P Pearlite
 q Quenchant
 s Start of transformation
 true True

REFERENCES

1. L. Huiping, Z. Guoqun, N. Shanting, and H. Chuanzhen: *Mater. Sci. Eng. A*, 2007, vols. 452–453, pp. 705–14.
2. S.H. Kang and Y.T. Im: *J. Mater. Process. Technol.*, 2007, vols. 192–193, pp. 381–90.
3. M. Eshraghi Kakhki, A. Kermanpur, and M.A. Golozar: *Model. Simul. Mater. Sci. Eng.*, 2009, vol. 17, p. 045007.
4. S. Denis, D. Farias, and A. Simon: *ISIJ Int.*, 1992, vol. 32, pp. 316–25.
5. D. Homberg: *Acta Mater.*, 1996, vol. 44, pp. 4375–85.
6. R. Thomas, M. Ganesa-Pillai, P.B. Aswath, K.L. Lawrence, and A. Haji-Sheikh: *Metall. Mater. Trans. A*, 1998, vol. 29A, pp. 1485–98.
7. P.R. Woodard, S. Chandrasekar, and H.T.Y. Yang: *Metall. Mater. Trans. B*, 1999, vol. 30B, pp. 815–22.
8. S. Serajzadeh: *J. Mater. Process. Technol.*, 2004, vol. 146, pp. 311–17.
9. S.H. Kang and Y.T. Im: *Metall. Mater. Trans. A*, 2005, vol. 36A, pp. 2315–25.
10. P. Carlone, G.S. Palazzo, and R. Pasquino: *Comput. Math. Appl.*, 2010, vol. 59, pp. 585–94.
11. W.P. Oliveira, M.A. Savi, P.M.C.L. Pacheco, and L.F.G. de Souza: *Mech. Mater.*, 2010, vol. 42, pp. 31–43.
12. J.S. Kirkaldy and D. Venugopalan: in *Phase Transformations in Ferrous Alloys*, A.R. Marder and J.I. Goldstein, eds., AIME, Warrendale, PA, 1983, pp. 125–48.
13. B. Buchmayr and J.S. Kirkaldy: *J. Heat. Treat.*, 1990, vol. 8, pp. 127–36.
14. D.F. Watt, L. Coon, M. Bibby, J. Goldak, and C. Henwood: *Acta Metall.*, 1998, vol. 36, pp. 3029–35.
15. T.C. Nguyen and D.C. Weckman: *Metall. Mater. Trans. B*, 2006, vol. 37B, pp. 275–92.
16. P. Akerstrom and M. Oldenburg: *J. Mater. Process. Technol.*, 2006, vol. 174, pp. 399–406.
17. V.M. Li, D.V. Niebuhr, L.L. Meekisho, and D.G. Atteridge: *Metall. Mater. Trans. B*, 1998, vol. 29B, pp. 661–72.
18. T.S. Prasanna Kumar: *Numer. Heat Transf. Part B*, 2004, vol. 45, pp. 541–63.
19. T.S. Prasanna Kumar and H.C. Kamath: *Metall. Mater. Trans. B*, 2004, vol. 35B, pp. 575–85.
20. K. Babu and T.S. Prasanna Kumar: *Metall. Mater. Trans. B*, 2010, vol. 41B, pp. 214–24.
21. K. Babu and T.S. Prasanna Kumar: *J. Heat Trans-T ASME*, 2011, vol. 133, 071501 (8 pages).
22. K. Babu and T.S. Prasanna Kumar: *Int. Heat Mass Transf.*, 2011, vol. 54, pp. 106–17.
23. D.P. Koistinen and R.E. Marburger: *Acta Metall.*, 1959, vol. 7, pp. 59–60.
24. C.H. Gur and J. Pan: *Handbook of Thermal Process Modeling of Steels*, Taylor & Francis Group, New York, 2008.
25. C.Y. Kung and J.J. Rayment: *Metall. Trans. A*, 1982, vol. 13A, pp. 328–31.
26. S.J. Lee and Y.K. Lee: *Mater. Des.*, 2008, vol. 29, pp. 1840–44.
27. K. Babu and T.S. Prasanna Kumar: ICTPMCS’10 ID No. C02, 2010, Shanghai, China.